Optical and Quantum Electronics (2020) 52:412
https://doi.org/10.1007/s11082-020-02526-y

High-speed thermally tuned electro-optical logic gates based on micro-ring resonators

Dias Azhigulov[1] · Bikash Nakarmi[2] · Ikechi Augustine Ukaegbu[1]

Received: 23 February 2020 / Accepted: 29 August 2020 / Published online: 11 September 2020

Abstract
This work proposes electro-optical design of logic gates using micro-ring resonators (MRR). We achieve this through various combinations of MRRs. In order to modulate the rings, thermo-optic effect is utilized. The reported devices are completely CMOS-compatible and can be fabricated using existing technologies. We also provide static responses to explain the device working principles. By plotting dynamic response spectra, the performance of each device is examined. The proposed logic elements are able to operate at 0.4 Mbps.

Keywords Logic gates · Micro-ring resonators · Silicon photonics · Thermo-optic effect

1 Introduction

Nowadays silicon photonics has been drawing the attention of researchers around the world as a potential candidate to replace electronic devices. Optical solutions offer a number of advantages over their electronic counterparts such as high speed, low inter-channel cross-talk, low electromagnetic interference (EMI), ability to carry several signals at once, and reduced power consumption (Miller 2000; Haurylau et al. 2006; Shacham et al. 2008).

For the past several decades, these useful properties were mainly utilized in the communication field to achieve ultrafast signal transmission (Caulfield and Dolev 2010). However, as recent discoveries show, optical devices are suitable for data processing as well. Some authors such as George et al. (2019) were able to design on-chip optical FFT by using delay lines. Additionally, standard complementary metal–oxide–semiconductor (CMOS) based

✉ Dias Azhigulov
dias.azhigulov@nu.edu.kz

✉ Ikechi Augustine Ukaegbu
ikechi.ukaegbu@nu.edu.kz

Bikash Nakarmi
bikash@nuaa.edu.cn

[1] Department of Electrical and Computer Engineering, Nazarbayev University, 010000 Nur-Sultan, Kazakhstan

[2] College of Electronic and Information Engineering, Nanjing University of Aeronautics and Astronautics, Nanjing, China

fabrication is being increasingly applied in optical device design. Consequently, this demonstrates that the field of silicon photonics matures and indeed provides a potential solution beyond Moore's Law.

To successfully implement an optical processing unit, it is necessary to start from the smallest logic elements, that is, from logic gates. While it is possible to build all-optical logic gates by mimicking the transistor-switched circuits, they are inherently limited by the accumulation of delays from cascading the gates. Thus, in order to avoid this, it is recommended to apply the concept of directed logics introduced by Hardy and Shamir (2007).

Directed logic is a paradigm shift that serves to utilize the full benefits of optics. Specifically, any operation here is performed using only one state delay since the inputs are fed in the form of vectors instead of Boolean scalars. To be precise, each switching element receives its input at the same time and depending on its value, performs the corresponding operation. These simple elements can be arranged in such a way as to perform a specific operation. The desired function will be computed within the state delay inherent to each switching element. Hence, there is no issue of cascaded delay, as each element does not have to wait for the preceding element to operate. Also, it is worth mentioning that such logic blocks compute both the function and its complement as well.

For optical switches, there are several options to consider. However, the two most prominent ones are micro-ring resonators (MRR) and Mach–Zehnder interferometers (MZI). To this date, a lot of research has been done on MZI based logic circuits (Ding et al. 2017; Reis et al. 2012; Kumar et al. 2014; El-Saeed et al. 2016). Both devices share the same advantages such as reconfigurability, low power consumption, and low latency. Yet, MZIs require large areas. In contrast, MRRs can be as compact as few micrometers and provide high data rates. Moreover, as reported in Gulde et al. (2005), the high refractive index contrast between silicon and an insulator greatly adds to the switching performance of MRRs. Therefore, they are more suitable for logic applications.

There are vast numbers of logic gates that are based on MRRs. To manipulate the switching process at high rates, most of the existing studies control the carrier density in the ring (Ibrahim et al. 2003; Yang et al. 2014). These methods are proven to work, yet we promote thermo-optic modulation schemes, as they are simple to fabricate and benefit from increased temperature sensitivity of silicon based MRRs (Ng et al. 2007). Tian et al. (2011) and Zhang et al. (2010) demonstrated that it is possible to achieve 10–20 kbps throughput in logic gates using the thermo-optic effect. We extended this number to 25 kbps in our previous work (Azhigulov et al. 2019), which was devoted to universal logic gates. This paper, however, presents the design of every logic gate with modulation speed up to 0.4 Mbps.

The paper is organized as follows. First, we investigate the principle of operation of MRRs and mathematically justify it in Sect. 2. In Sect. 3, through a combination of qualitative and quantitative analysis, the designs of logic gates are explored. The first half of Sect. 4 discusses the static response spectra of the devices and suggests working wavelengths. Then, the dynamic behavior of the proposed devices is evaluated by comparing the results to the expected outputs. Finally, in Sect. 5, we summarize and conclude our work.

2 Micro-ring resonator as a switching element

2.1 Operation principle

A conventional add-drop ring resonator is composed of two straight waveguides accompanied by a ring cavity. As depicted in Fig. 1, it has four ports in total, namely, input port, through port, add port, and drop port. We configure the resonator such that the constant wavelength (CW) light enters from the input port, though other options are possible. Thus, the light confined in the upper waveguide couples with the ring cavity only if the length of the round-trip path is an integer multiple of the wavelength of the light. Mathematically, this can be expressed as (Bogaerts et al. 2011):

$$\lambda_{res} = \frac{n_{eff} L}{m}, \quad m = 1, 2, 3 \ldots \tag{1}$$

where λ_{res} is the resonant wavelength, n_{eff} is the effective refractive index of the waveguide, L is the circumference of the ring, and m is the mode number. If the input optical signal has a wavelength that is not integer multiple of the round-trip path, the signal passes by the ring cavity and makes its way at the through port. In other words, the CW light has to have the same wavelength as the resonant wavelength of MRR in order for coupling to occur. Note that whenever the light gets coupled with the ring cavity, it appears at drop port of the device. Also, it could be noticed that the output of the through port is an inverse of the drop port. This feature enables MRR-based devices to perform the desired function and its complement too.

The intensity of the signal at the through and drop ports is given as (Heebner et al. 2008):

$$T_{through} = \frac{r_2^2 a^2 - 2 r_1 r_2 a * cos\phi + r_1^2}{1 - 2 r_1 r_2 a * cos\phi + \left(r_1 r_2 a\right)^2} \tag{2}$$

$$T_{drop} = \frac{a\left(1 - r_1^2\right)\left(1 - r_2^2\right)}{1 - 2 r_1 r_2 a * cos\phi + \left(r_1 r_2 a\right)^2} \tag{3}$$

where r_1 and r_2 are the self-coupling coefficients, a and ϕ are the single-pass amplitude transmission and phase shift, respectively.

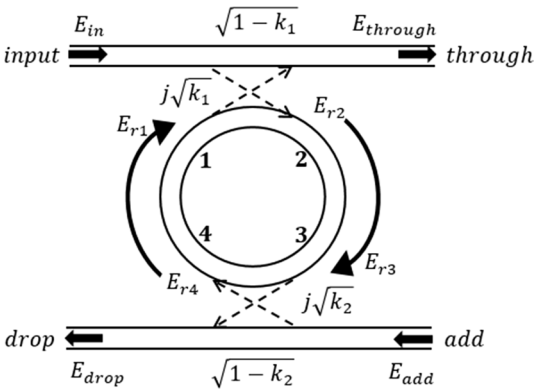

Fig. 1 Simple add-drop micro-ring resonator structure

2.2 Switching action

To design the structures, Lumerical DEVICE simulation software was employed. Each MRR features a compact micro-heater placed on top. The micro-heaters are made of nickel chromate and are omega-shaped (Fig. 2), for it facilitates heat distribution (Geuzebroek et al. 2003). Then, by placing gold contacts on top of the heaters we create a two-terminal device. It can be turned on and off through voltage variations across the terminals.

In general, the temperature difference Δt across the ring cavity leads to a change in its effective refractive index Δn_{eff} (Xu et al. 2019). Our simulations are based on the assumption of linear relationship between temperature and effective refractive index for the temperature range 300–350 K (refer to Fig. 14), Furthermore, a shift in n_{eff} affects the resonant wavelength based on the expression below (Geuzebroek et al. 2003):

$$\frac{\Delta n_{eff}\,\lambda}{n_{eff}} \approx \delta\lambda \tag{4}$$

From (4), $\delta\lambda$ is the shift in resonant wavelength of the device. It should be emphasized that in this work, MRR is switched off (decoupled) by default. Consequently, for coupling (switch on) to occur, it is necessary to change its λ_{res} to be identical to that of the input CW light. As discussed above, this can be accomplished by varying the temperature. Conversely, if we cease heating, in a short window of time, λ_{res} returns to its original value thereby decoupling (switch off) the device. Such two wavelengths based approach is commonly used in the literature (Tian et al. 2016, 2017; Bharti et al. 2019). This fundamental switching action is applied across all the proposed devices.

3 Device design

3.1 Truth tables

Below are the truth tables for the logic gates discussed in this work. It should be noted that NOT gate is omitted in the tables as well as in design since it is fairly simple and can be constructed using a single MRR.

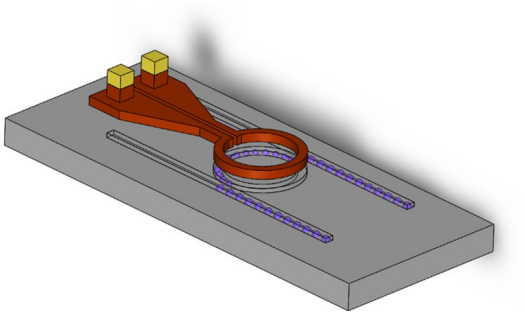

Fig. 2 The microheater placed on top of MRR. The purple spheres represent the light passing through the resonator

3.2 Quantitative analysis

In order to completely understand the workflow of the electro-optical gates, one should become acquainted with relevant analytical formulations. As illustrated in Fig. 1, electric fields at the input and add ports are given as E_{in} and E_{add}, respectively. $E_{through}$ is the electric field at the through port, whereas E_{drop} denotes the drop port electric field. Furthermore, there are additional notations for the fields in the ring cavity at points 1, 2, 3, and 4, as shown in Fig. 1. The fields at each of these points, namely 1, 2, 3, and 4, are given as E_{r1}, E_{r2}, E_{r3}, and E_{r4}, respectively, and the expression for each of them is given as (Rakshit et al. 2012):

$$E_{r1} = \sqrt{1-\gamma} * \left[j\sqrt{k_1} * E_{in} + \sqrt{1-k_1} * E_{r4} \right] \tag{5}$$

$$E_{r2} = E_{r1} * e^{-\frac{\alpha L}{4}} e^{jk_n * \frac{L}{2}} \tag{6}$$

$$E_{r3} = \sqrt{1-\gamma} * \left[j\sqrt{k_2} * E_{add} + \sqrt{1-k_2} * E_{r2} \right] \tag{7}$$

$$E_{r4} = E_{r3} * e^{-\frac{\alpha L}{4}} e^{jk_n * \frac{L}{2}} \tag{8}$$

where k_1 and k_2 are the cross-coupling coefficients, γ is the intensity loss coefficient of the couplers, α is the intensity attenuation coefficient of the ring, and k_n is the wave propagation constant. Then, electric fields at the through and drop ports can be written as:

$$E_{through} = \sqrt{1-\gamma} * \left[\sqrt{1-k_1} E_{in} + j\sqrt{k_1} * E_{r4} \right] \tag{9}$$

$$E_{drop} = \sqrt{1-\gamma} * \left[\sqrt{1-k_2} * E_{add} + j\sqrt{k_2} * E_{r2} \right] \tag{10}$$

After expressing E_{r4} and E_{r2} in terms of E_{in} and E_{add}, they can be replaced in (9) and (10):

$$E_{through} = \frac{\sqrt{1-k_1} - \sqrt{1-k_2} * e^{-\frac{\alpha L}{2}} e^{j2\varphi}}{1 - \sqrt{1-k_1}\sqrt{1-k_2} * e^{-\frac{\alpha L}{2}} e^{j2\varphi}} E_{in} - \frac{\sqrt{k_1 k_2} * e^{-\frac{\alpha L}{4}} e^{j\varphi}}{1 - \sqrt{1-k_1}\sqrt{1-k_2} * e^{-\frac{\alpha L}{2}} e^{j2\varphi}} E_{add} \tag{11}$$

$$E_{drop} = \frac{-\sqrt{k_1 k_2} * e^{-\frac{\alpha L}{4}} e^{j\varphi}}{1 - \sqrt{1-k_1}\sqrt{1-k_2} * e^{-\frac{\alpha L}{2}} e^{j2\varphi}} E_{in} + \frac{\sqrt{1-k_2} - \sqrt{1-k_1} * e^{-\frac{\alpha L}{2}} e^{j2\varphi}}{1 - \sqrt{1-k_1}\sqrt{1-k_2} * e^{-\frac{\alpha L}{2}} e^{j2\varphi}} E_{add} \tag{12}$$

It should be noted that Eqs. (11) and (12) hold true under the assumption that there is the lossless coupling between the ring cavity and the waveguides (i.e. $\gamma = 0$). We can find the signal power at each port by squaring their respective electric fields ($P \propto E^2$). These equations prove useful when it comes to device design and in particular when considering the cascaded effects of MRRs.

3.3 Qualitative analysis

Figure 3 represents the structure of the device exhibiting the properties of OR/NOR gates simultaneously. The MRRs are configured in parallel for logic to work. The radius of each ring is set to be 10 μm and the coupling gap is 0.2 μm. The rings are shaped in the form of racetracks in order to increase the coupling capability of the structures. Specifically, the coupling length is 6 μm. The device is built according to the standard silicon-on-insulator (SOI) formation. To modulate the CW light, Electrical Pulse Sequence (EPS) is employed. Thus, a binary sequence of input signals A and B are carried out in the electrical domain. They are applied to micro-heaters in order to modulate the incoming light. Hence, there are two separate micro-heaters placed on top of each MRR. EPS A is applied to the first heater, whereas EPS B belongs to the second one. These electrical signals are produced by a non-return-to-zero (NRZ) pulse generator. The constant optical source is connected to the input port of the device to project the light into the upper waveguide. It can be noticed that the input signals are of electrical type whereas the output of the device is computed in the optical domain.

The workflow of the device is simple: NOR logic is downloaded at the through port of the second MRR, while the drop port of MRR1 outputs OR logic. It is assumed that there is no light in the add port of MRR2. According to the schematics, the through port of the device (NOR) transmits logic 1 (high intensity optical signal) only if both rings are decoupled (i.e. $A=0$, $B=0$). Hence the logic is validated. Otherwise, each time the CW light becomes coupled with either of the MRRs, it will be downloaded at the drop port thereby proving the OR logic. Specifically, when at least one of the inputs becomes high (logic 1) there would be a shift in resonant wavelength of the ring. Therefore, under sufficient thermal disturbance, the wavelength of the CW light will match with that of the ring and thus, allowing the optical signal to travel through the ring cavity.

XOR/XNOR logics are obtained in a similar fashion albeit some changes in the design. In this case, the add port of the second MRR is tied to the drop port of the first one. This enables the device to execute XOR operation. In this design, the add port of the first MRR is assumed to be idle (i.e. no light transmission).

Note that no changes were introduced to the device structure in terms of dimensions. The core parameters such as the coupling coefficient were not altered as well. In fact, the only difference here is the addition of bending waveguides, which have a bend radius of 5 μm.

Based on the same approach as the OR/NOR case, it can be seen that XOR output transmits nonzero optical signal only when either of the MRRs is switched on (Fig. 4). Conversely, if identical signals are applied to both MRRs, XNOR output becomes high. This shows that both logics hold true for the device under consideration.

In comparison to the previous two structures, AND/NAND logics arrangement connects the MRRs in series. Moreover, this design is perhaps the most complex one as it consists

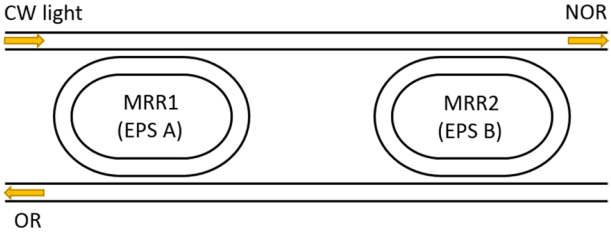

Fig. 3 Design of the device executing OR/NOR logic operations

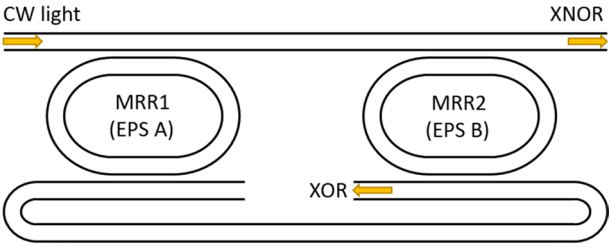

Fig. 4 Design of the device executing XOR/XNOR logic operations

of the bending waveguides of the same radius of 5 μm and a Y-coupler. Furthermore, the MRR design is slightly changed—the coupling length of each ring is set to be 4 μm.

As portrayed in Fig. 5, the series combination of the resonators results in the AND operation. Because for this port to be high, both resonators should have the resonant wavelengths equal to that of the CW light (i.e. switched on). In any other case, the light will travel to the Y-coupler and exit through the NAND port. Therefore, the device concurrently exhibits the properties of AND/NAND logic gates. Similar to the previous configuration (XOR/XNOR), we do not use the add port of the first MRR.

4 Results

4.1 Static response

Static response is a useful means to visualize the behavior of the devices under various conditions. Moreover, it alleviates the selection of wavelength for CW light. In order to obtain static response, the setup illustrated in Fig. 6 was implemented in Lumerical INTERCONNECT. Optical Network Analyzer (ONA) outputs the CW light to the input port of the Device Under Test (DUT) and simultaneously reads optical signals from two ports of the device. In order to evaluate each binary combination of inputs, DC Sources' values should be varied for every scenario. DC Source 1 emulates A, and DC Source 2 emulates B from truth tables. For brevity reasons, the response spectra were plotted for

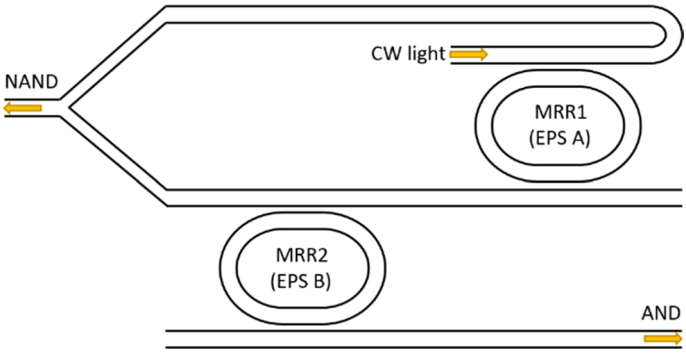

Fig. 5 Design of the device executing AND/NAND logic operations

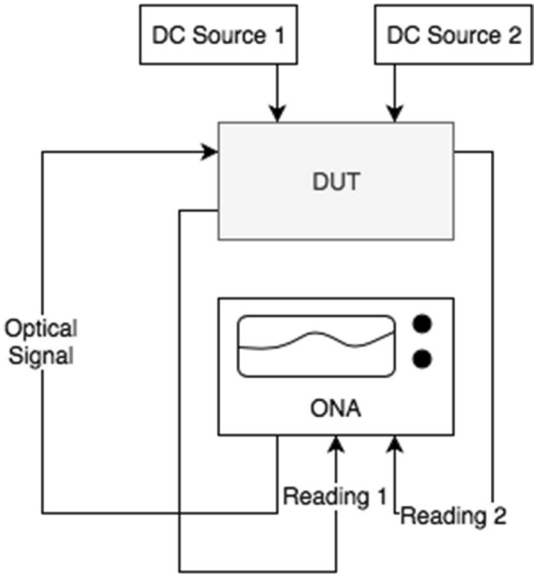

Fig. 6 Setup for static response test. *ONA* optical network analyzer, *DUT* device under test

through port transmission only. However, one can expect similar but opposite patterns for drop port since the signal, which does not come out of the through port, appears at the drop port.

We apply 20 mW power to each micro-heater to create a noticeable change in the refractive indices of the resonators. Figures 7, 8 and 9 depict the static response spectra at the through port of each device. In other words, only NOR, XNOR, and NAND gates' static responses are provided since adding the plots for their respective complements is superfluous as the pattern will merely be the opposite of what is presented in Figs. 7, 8 and 9.

Thus, referring to Fig. 7, the working wavelength of 1545.06 nm was chosen for the first device in order to obtain an optimal extinction ratio. At this particular point, we have the largest resonant dips for three cases of OR/NOR (A, B = 0; A = 0 and B = 1; A = 1 and

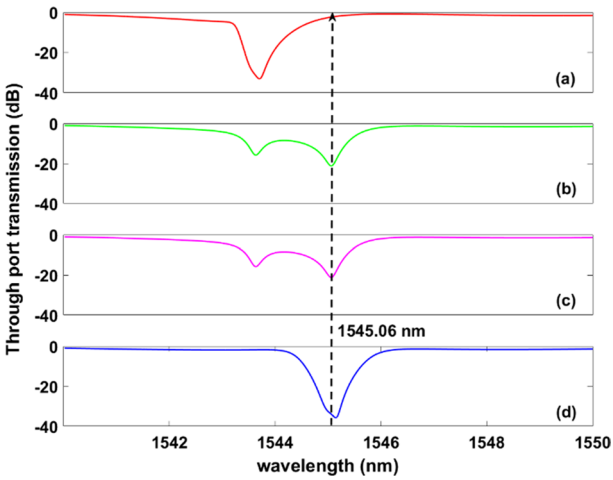

Fig. 7 Static response spectra of the OR/NOR logics circuit. **a** Both MRRs are off; **b** MRR1 is off and MRR2 is on; **c** MRR1 is on and MRR2 is off; **d** both MRRs are on

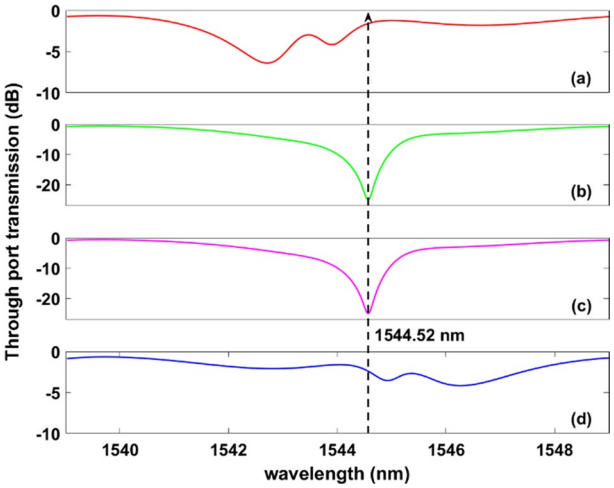

Fig. 8 Static response spectra of the XOR/XNOR logics circuit. **a** Both MRRs are off; **b** MRR1 is off and MRR2 is on; **c** MRR1 is on and MRR2 is off; **d** both MRRs are on

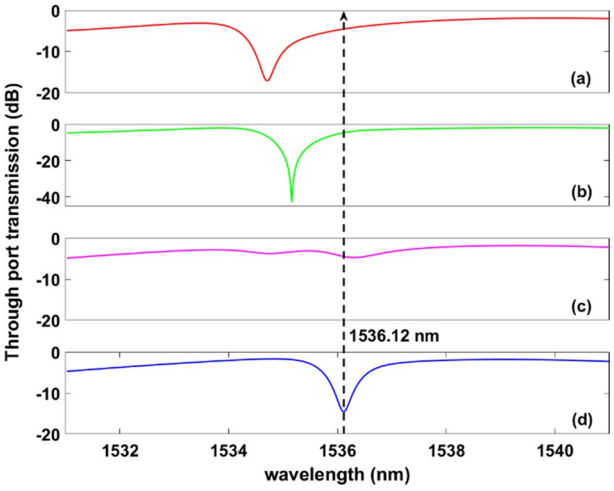

Fig. 9 Static response spectra of the AND/NAND logics circuit. **a** Both MRRs are off; **b** MRR1 is off and MRR2 is on; **c** MRR1 is on and MRR2 is off; **d** both MRRs are on

Table 1 The truth table of the device performing OR/NOR operations

A	B	OR	NOR
0	0	0	1
0	1	1	0
1	0	1	0
1	1	1	0

B = 0) from Table 1. Figure 7a demonstrates the gain at the through port (i.e. NOR port output) when both inputs (A and B) are zero. 0 dB gain in the graphs corresponds to the complete transmission of the CW light without any losses. Consequently, it can be noticed that for the first case the optical high signal appears at the through port of the OR/NOR logic device. Figure 7b and c indicate the gain when either B = 1 or A = 1, respectively.

Table 2 The truth table of the device performing AND/NAND operations

A	B	AND	NAND
0	0	0	1
0	1	0	1
1	0	0	1
1	1	1	0

Table 3 The truth table of the device performing XOR/XNOR operations

A	B	XOR	XNOR
0	0	0	1
0	1	1	0
1	0	1	0
1	1	0	1

The plots look identical because of the symmetrical structure of the device. Also, there are two distinct dips with each being half as small as in the case of Fig. 7a. They are at different wavelengths indicating that only one MRR is heated (active). To be precise, the active resonator has its resonant dip shifted to 1545.06 nm, while the other one preserves its state thereby introducing another resonant dip at the original position (~ 1543.62 nm). Because of the significant drops in the output optical signal, it can be confirmed that when either of the inputs is high, optical low signal is transmitted at the through port. The last case is when both A and B are equal to 1 (Fig. 7d). The resonant wavelengths of the MRR1 as well as MRR2 shift to 1545.06 nm. As a result, the light can be coupled with both resonators, producing a sharp drop in gain at the through port. Again, this implies that there is no optical signal present at the NOR port, which is equivalent to optical 0. Consequently, the signal is at the opposite end of the device (i.e. OR port) and therefore, optical 1 can be observed at the OR port. Similar reasoning applies to all other cases. In essence, these four graphs imply that at this working wavelength it is possible to obtain OR/NOR logic functions with high extinction ratio of up to 20 dB.

Figure 8 represents the static response spectrum of the second proposed device. Similar to the previous case, here we have identical patterns for the inputs A = 0, B = 1 (Fig. 8b) and A = 1, B = 0 (Fig. 8c). The reason is that the overall device structure did not experience significant changes and thus, remains symmetrical. The working wavelength was decided to be 1544.52 nm for sharper differences between output logic high and low signals. This yielded in 22.5 dB extinction ratio: 25 dB dips are observed in the case when only one of the MRRs is on (i.e. at resonant state), which is indicative of the optical low signal at the XNOR output; if both MRRs have the same state (Fig. 8a and d), the optical high signal can be observed at the through port (i.e. XNOR), diminishing the loss down to 2.48 dB. In this way, we verified the logic (Table 2).

The last device's static response is depicted in Fig. 9. The working wavelength was configured to be at 1536.12 nm, for it offers the greatest extinction ratio. As it was defined in Table 3, for AND logic one requires both input signals to be high in order to obtain nonzero signal at the output. According to Fig. 9, this is the case with the proposed design as the optical high signal appears at the through port (NAND) of the device for the three following cases: A, B = 0; A = 0 and B = 1; A = 1 and B = 0. Only when both input signals

are high does the NAND port experience substantial drops in signal level (Fig. 9d), which implies that the optical high signal is detected at the AND port. Therefore, one can deduce that the device successfully executes AND/NAND logic operations. The extinction ratio constitutes 10.6 dB.

An important observation from Fig. 9c is that there are no clear resonant dips relative to other cases. This may be due to asymmetry in the design. In fact, from Fig. 5 one can notice that there are two possible paths for the optical signal to reach the NAND port. This is the case in Fig. 9c where the light couples with the first MRR and then passes by through the second one. Despite MRR2 being inactive, nonzero coupling length of the ring cavity introduces noticeable losses. Furthermore, the Y-coupler itself contributes to the performance degradation of the device by introducing additional losses.

4.2 Dynamic response

Having determined the working wavelengths for each device, we can analyze the dynamic behavior of the devices. Specifically, we measure the signal at relevant ports of the devices and plot the output with respect to time. Therefore, unlike in static response, inputs A and B will vary with time. To realize this, we connected CW laser with 1 mW power to the input port of each device. Afterward, using NRZ pulse generators, voltage differences were created according to the input bit sequence (Fig. 10). The results are plotted in Figs. 11, 12 and 13.

Thus, we were able to consistently achieve 0.4 Mbps modulation of each MRR with thermal tuning. The upper limit on the operation speed was derived based on the performance of a single MRR. According to Eq. (4), for thermally tuned MRR with $\Delta n_{eff}/\Delta t = 2.04*10^{-4}$ (Fig. 14), the desired wavelength shift becomes 0.1294 nm/K, which in turn, suggests $\Delta t = 11.6$ K to obtain 1.5 nm shift in resonant wavelength. Note that 1.5 nm is the distance between two resonant states across all devices. However, as illustrated in Fig. 15, the true temperature shift required is 20 K. This mismatch occurs due to the fact that Eq. (4) is an approximation of the relationship between wavelength shift and change in the effective refractive index of silicon. We further conduct heat simulation of the MRR to illustrate its thermal behavior with time. Figure 16 demonstrates the heating and corresponding cooling rates for the MRR. Thus, 2.5 µs is enough to elevate the temperature to 320 K, which confirms our results. Furthermore, the device requires only 1.25 µs to cool down to the initial conditions as indicated in Fig. 17. To be precise, at 1.25 µs, the MRR's temperature reaches 302 K (Fig. 16) and by referring to Fig. 15, it can be deduced that this temperature is sufficient for the resonator to return to the original state. This is not the case with heating stage because the two resonant wavelengths have to be separated far away (1.5 nm is optimum) in order to have the highest extinction ratio.

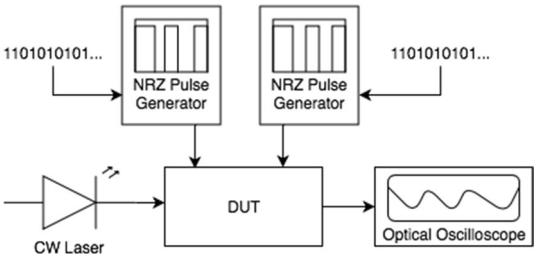

Fig. 10 Simulation setup for dynamic response test

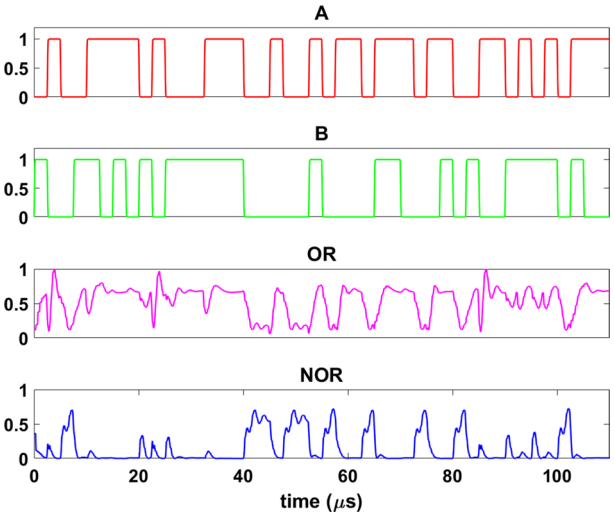

Fig. 11 Dynamic response of the first logic unit at 0.4 Mbps input stream

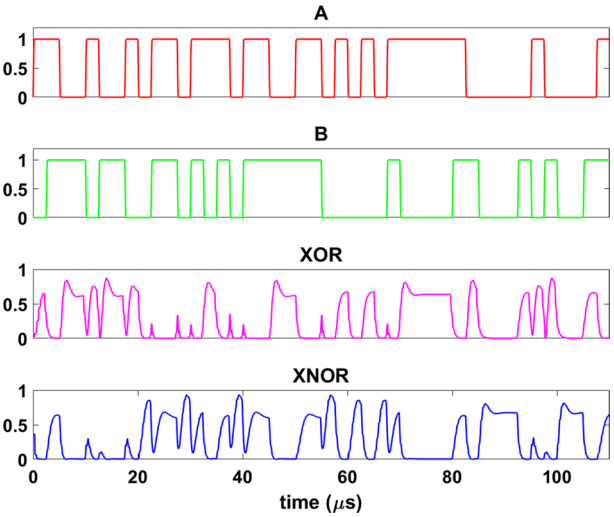

Fig. 12 Dynamic response of the second logic unit at 0.4 Mbps input stream

Note that the outputs of every device were normalized with respect to their input optical power levels. Some short spikes can be observed in the outputs of all devices (Figs. 11, 12, 13). These are caused by the inputs' transition states, that is, when both inputs are simultaneously transitioning from one state to another. Additionally, inconsistencies in logic high levels of the XNOR port can be noticed. The reason is that these logic highs are triggered by different combinations of inputs. Therefore, the light travels through different paths to get to the output. There are also certain bias levels at the outputs OR, AND as well as NAND. The first two are explained by the fact that in all cases, the light travels close to the ring cavities, and due to the increased coupling length, a portion of light escapes to other ports. As a result, this produces nonzero readings at the outputs where 0 is expected. While this is true, it is also the case that during the resonant coupling process, a modicum of light will not be coupled due to structural non-idealities as well as the lossy environment. As

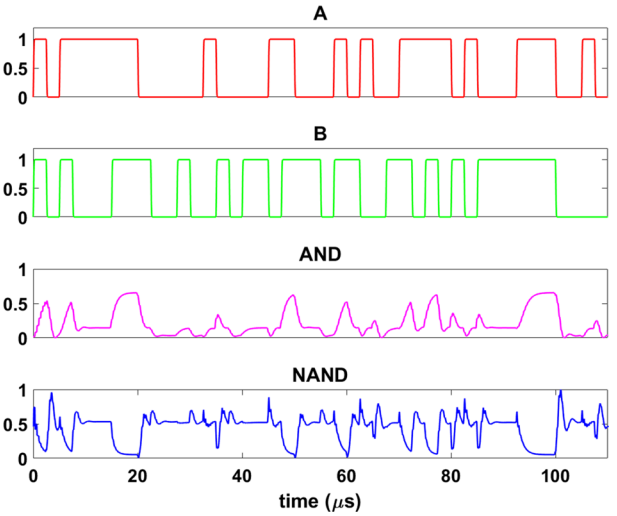

Fig. 13 Dynamic response of the third logic unit at 0.4 Mbps input stream

Fig. 14 Effective refractive index of silicon as a function of temperature

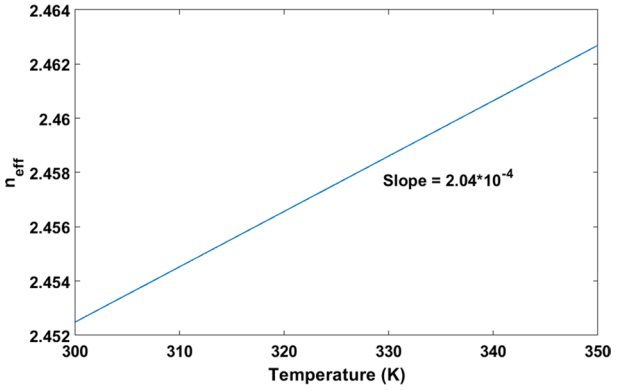

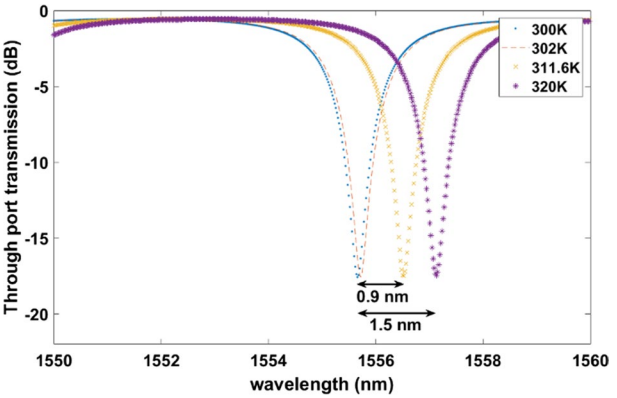

Fig. 15 Static response of the simulated MRR at four temperature values

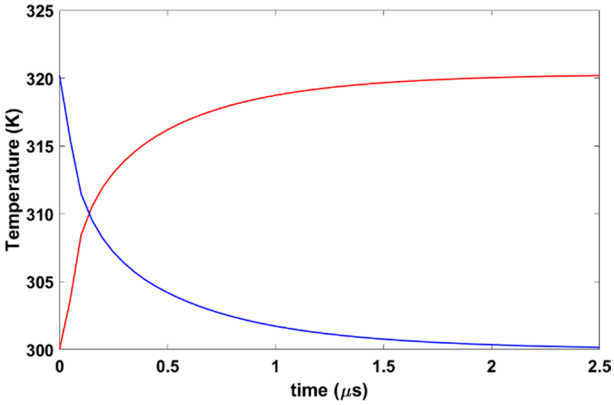

Fig. 16 Thermal dynamics of the simulated MRR. Red curve depicts the heating phase (20 mW applied), whereas blue curve stands for the cooling part

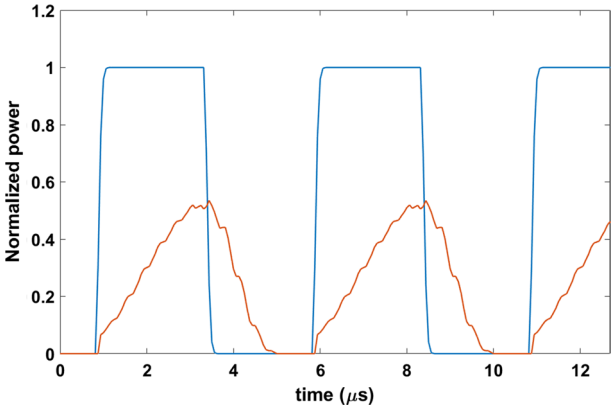

Fig. 17 Dynamic response of the simulated MRR at 0.4 Mbps. Blue lines are the electrical input pulses and the orange waveform is the optical output downloaded at the drop port of the device

such, the part which does not couple with the rings travels to the other port. Therefore, we observe some bias at the NAND output.

Another issue to mention is the reduced signal levels at AND/NAND gates. Again, as discussed in the first part of the section, we reason that this is because of the increased path lengths as well as due to Y-coupler losses. Undesired coupling between the light and the ring cavities is also a factor. Despite these non-idealities, it can be claimed that all the proposed devices successfully function as logic gates.

5 Conclusion

In this paper, we presented a set of photonic devices performing all basic logic gates. In order to implement the electro-optical logic gates, we applied the directed logic principle. MRRs were modulated using the thermo-optic effect of silicon. By selecting a suitable working wavelength and setting up all the simulation pipeline, static and dynamic response spectra were plotted. Following our analysis, some non-idealities were identified in device behavior and addressed accordingly. With the proposed design, we were able to perform modulation at a high speed of 0.4 Mbps for each device. Future works can be done on

the design regarding the modulation scheme. Other modulation techniques can be realized for very high-speed applications. Additionally, the device footprint can be further reduced through design optimization and ring radius decrease.

Acknowledgements This work was supported by Nazarbayev University (064.01.00).

References

Azhigulov, D., Ukaegbu, I., Park, H.: The design of universal logic gates using microring resonator structures. In: Physics and Simulation of Optoelectronic Devices XXVII, pp. 155–161 (2019)

Bharti, G.K., Biswas, U., Rakshit, J.K.: Design of micro-ring resonator based all optical universal reconfigurable logic circuit. Optoelectron. Adv. Mater. Rapid Commun. **13**(7–8), 407–414 (2019)

Bogaerts, W., et al.: Silicon microring resonators. Laser Photonics Rev. **6**(1), 47–73 (2011). https://doi.org/10.1002/lpor.201100017

Caulfield, H., Dolev, S.: Why future supercomputing requires optics. Nat. Photonics **4**(5), 261–263 (2010). https://doi.org/10.1038/nphoton.2010.94

Ding, J., Yang, L., Chen, Q., Zhang, L., Zhou, P.: Demonstration of a directed XNOR/XOR optical logic circuit based on silicon Mach-Zehnder interferometer. Opt. Commun. **395**, 183–187 (2017). https://doi.org/10.1016/j.optcom.2015.08.024

El-Saeed, E., El-Aziz, A., Fayed, H., Aly, M.: Optical logic gates based on semiconductor optical amplifier Mach-Zehnder interferometer: design and simulation. Opt. Eng. **55**(2), 025104 (2016). https://doi.org/10.1117/1.oe.55.2.025104

George, J.K., Nejadriahi, H., Sorger, V.J.: Towards on-chip optical FFTs for convolutional neural networks. In: 2017 IEEE International Conference on Rebooting Computing (ICRC), Washington, DC, 2017, pp. 1–4 (2019). https://doi.org/10.1109/icrc.2017.8123675

Geuzebroek, D.H., Klein, E.J., Kelderman, H., Driessen, A.: Wavelength tuning and switching of a thermo-optic microring resonator. In: The 11th ECIO Conference, Prague (2003)

Gulde, S., Jebali, A., Moll, N.: Optimization of ultrafast all-optical resonator switching. Opt. Express **13**(23), 9502 (2005). https://doi.org/10.1364/opex.13.009502

Hardy, J., Shamir, J.: Optics inspired logic architecture. Opt. Express **15**(1), 150 (2007). https://doi.org/10.1364/oe.15.000150

Haurylau, M., et al.: On-chip optical interconnect roadmap: challenges and critical directions. IEEE J. Sel. Topics Quantum Electron. **12**(6), 1699–1705 (2006). https://doi.org/10.1109/jstqe.2006.880615

Heebner, J., Grover, R., Ibrahim, T.: Optical Microresonators, pp. 84–85. Springer, London (2008)

Ibrahim, T., Grover, R., Kuo, L., Kanakaraju, S., Calhoun, L., Ho, P.: All-optical AND/NAND logic gates using semiconductor microresonators. IEEE Photonics Technol. Lett. **15**(10), 1422–1424 (2003). https://doi.org/10.1109/lpt.2003.818049

Kumar, A., Kumar, S., Raghuwanshi, S.: Implementation of XOR/XNOR and AND logic gates by using Mach–Zehnder interferometers. Optik **125**(19), 5764–5767 (2014). https://doi.org/10.1016/j.ijleo.2014.07.037

Miller, D.: Rationale and challenges for optical interconnects to electronic chips. Proc. IEEE **88**(6), 728–749 (2000). https://doi.org/10.1109/5.867687

Ng, H., et al.: Wavelength reconfigurable photonic switch using thermally tuned microring resonators fabricated on silicon substrate. IEEE Photonics Technol. Lett. **19**(9), 704–706 (2007). https://doi.org/10.1109/lpt.2007.895420

Rakshit, J.K., Roy, J.N., Chattopadhyay, T.: All-optical XOR/XNOR logic gate using micro-ring resonators. In: 5th International Conference on Computers and Devices for Communication (CODEC), Hyatt Regency Kolkata (2012)

Reis, C., Chattopadhyay, T., André, P., Teixeira, A.: Single Mach-Zehnder interferometer based optical Boolean logic gates. Appl. Opt. **51**(36), 8693 (2012). https://doi.org/10.1364/ao.51.008693

Shacham, A., Bergman, K., Carloni, L.: Photonic networks-on-chip for future generations of chip multiprocessors. IEEE Trans. Comput. **57**(9), 1246–1260 (2008). https://doi.org/10.1109/tc.2008.78

Tian, Y., et al.: Proof of concept of directed OR/NOR and AND/NAND logic circuit consisting of two parallel microring resonators. Opt. Lett. **36**(9), 1650 (2011). https://doi.org/10.1364/ol.36.001650

Tian, Y., et al.: Reconfigurable electro-optic logic circuits using microring resonator-based optical switch array. IEEE Photonics J. **8**(2), 1–8 (2016)

Tian, Y., et al.: Experimental demonstration of a reconfigurable electro-optic directed logic circuit using cascaded carrier-injection micro-ring resonators. Sci. Rep. **7**(1), 1–10 (2017)
Xu, D.-X., Delâge, A., Verly, P., Janz, S., Wang, S., Vachon, M., Ma, P., Lapointe, J., Melati, D., Cheben, P., Schmid, J.H.: Empirical model for the temperature dependence of silicon refractive index from O to C band based on waveguide measurements. Opt. Express **27**, 27229–27241 (2019)
Yang, L., Zhang, L., Guo, C., Ding, J.: XOR and XNOR operations at 12.5 Gb/s using cascaded carrier-depletion microring resonators. Opt. Express **22**(3), 2996 (2014). https://doi.org/10.1364/oe.22.002996
Zhang, L., et al.: Demonstration of directed XOR/XNOR logic gates using two cascaded microring resonators. Opt. Lett. **35**(10), 1620 (2010). https://doi.org/10.1364/ol.35.001620